Multiaxial Prestress of Reinforced Concrete I-Beams

Fernando Fraternali*, Bruno Palazzo**, Gerardo Carpentieri***

SUMMARY – *We analyze the effects of multiaxial prestress on the limit behavior of I-shaped reinforced concrete elements subjected to combined axial load and bending. We provide a collection of design charts and moment – curvature diagrams for reinforced concrete I-beams with laterally and longitudinally prestressed flanges. The given results highlight the special ability of the active prestress technique in enhancing the strength and ductility properties of seismic resistant columns and shear walls.*

Keywords: lateral prestress, I-beams, prestressed reinforced concrete, strength domains, moment-curvature diagrams, structural ductility.

1. **Introduction**

The lateral confinement of reinforced concrete (RC) elements through pre-heated steel rings, ordinary stirrup reinforcements, and/or Fiber-Reinforced Polymer (FRP) wraps are well known strengthening techniques in the field of construction industry. Such reinforcement methods are able to transform the uniaxial state of stress of an unconfined element, which is subject to axial loading and bending, into a multiaxial state of stress, due to the restraining pressure applied by the transverse reinforcement. The latter may appreciably increase the material strength, by moving Mohr's stress circles towards the compression region of the intrinsic strength curve (Fig. 1).

The "passive" confinement of RC elements is mainly effective in presence of large axial strains (i.e., in correspondence with axial stresses approaching the concrete uniaxial strength), and less effective under small axial strains, due to low Poisson's ratios of common concretes. More challenging is the "active" confinement of I-shaped RC members, which is obtained by laterally prestressing the terminal flanges (Fig. 2). Such a prestressing technique is well suited for seismic resistant RC columns or shear walls, where the presence of bi-axial/tri-axial compression states may significantly enhance strength and ductility properties of the element (Fig. 3).

[Gardener et al., 1992] present an experimental and theoretical study on the load capacity of laterally compressed RC columns subjected to eccentric axial forces, formulating an empirical formula to predict the ultimate load of such elements. [Zaki, 2013] studies the optimal design of external FRP confinements of RC columns subject to axial and bending loads, determining optimized values of the FRP wrapping thickness and lengths. [Saadatmanesh et al., 1997] present an experimental study on the repair though FRP wraps of earthquake damaged RC columns. The FRP reinforced columns examined in such a study show enhanced hysteretic response, flexural strength and displacement ductility, as compared to the original elements. [Janke et al., 2009] investigate on the compression behavior of cylindrical concrete elements reinforced with prestressed steel and carbon FRP wraps. The outcomes of this study show that the residual capacity of the elements reinforced with prestressed confinements is significantly higher than that of elements reinforced with unstressed wraps, even in presence of moderate confinement prestress. The strengthening and rehabilitation of RC members through external wrapping with prestressed FRP elements is investigated by [Mortazavi et al., 2003] and [Mukherjee and Rai, 2009]. Such studies show that the prestressing of confinement wraps and laminates significantly enhances the utilization of FRP materials and the concrete response [Mortazavi et al., 2003], as well as the design and ultimate loads (by

* Department of Civil Engineering, University of Salerno, Fisciano (SA), Italy, f.fraternali@unisa.it
** Department of Civil Engineering, University of Salerno, Fisciano (SA), Italy, palazzo@unisa.it
*** Department of Civil Engineering, University of Salerno, Fisciano (SA), Italy, gcarpentieri@unisa.it

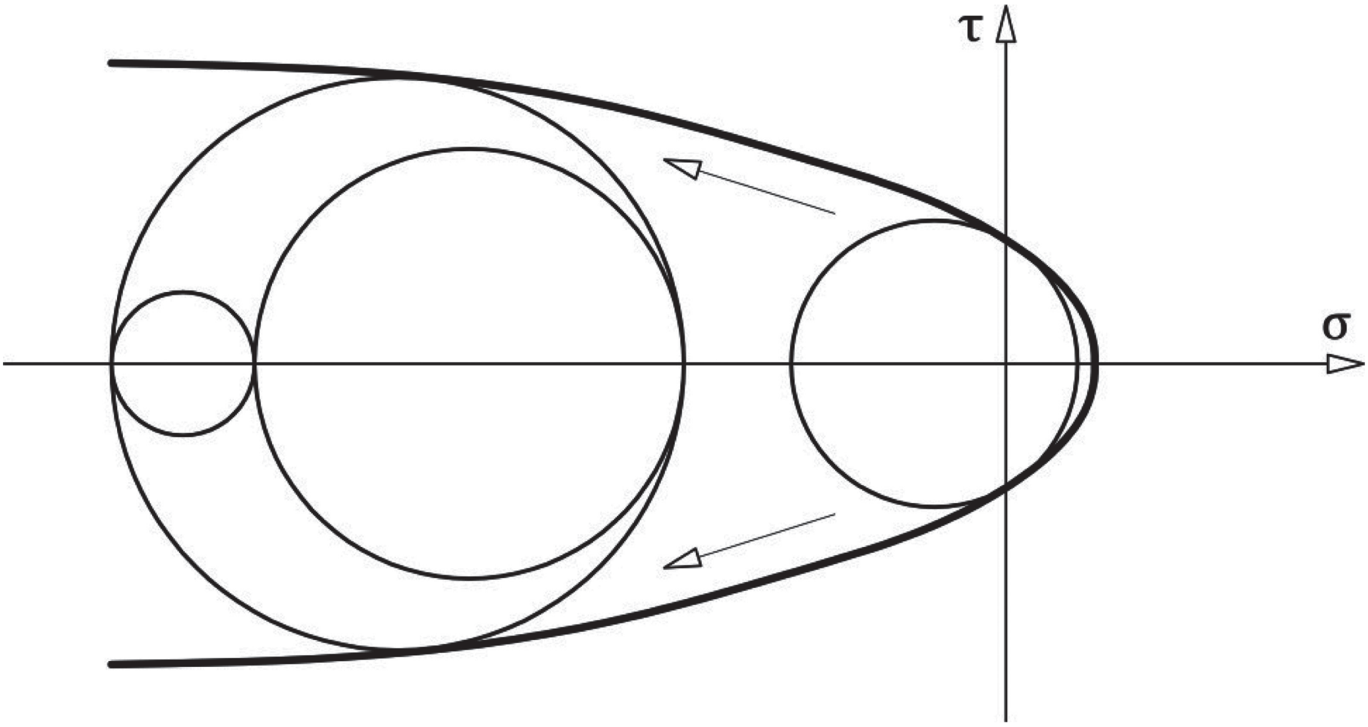

Fig. 1. *Strengthening effect of lateral prestress in brittle materials: shifting of Mohr circles towards the compression region (left) of the intrinsic strength curve.*
Effetti della precompressione laterale su materiali fragili: traslazione dei cerchi di Mohr verso la regione delle compressioni (sinistra) della superficie di resistenza intrinseca.

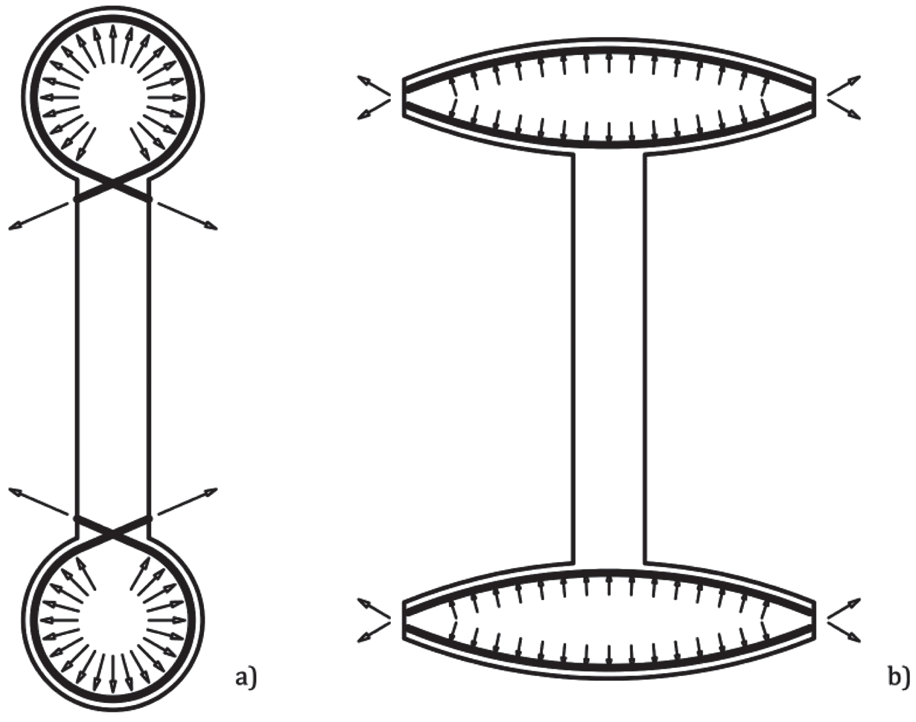

Fig. 2. *Active lateral prestress of the flanges of I-beams.*
Precompressione laterale attiva delle flange di travi a doppio T.

more than 100%) of FRC rehabilitated beams [Mukherjee and Rai, 2009].

The present work examines the ultimate limit state design of RC I-beams featuring 3D prestressed flanges, and subject to combined axial loads and bending moments. We deal with a parametric study on the strength domains and moment-curvature diagrams of such elements, on examining different aspect ratios, prestress levels, and steel reinforcement ratios. Our final goal is to show the effects of such design variables on the

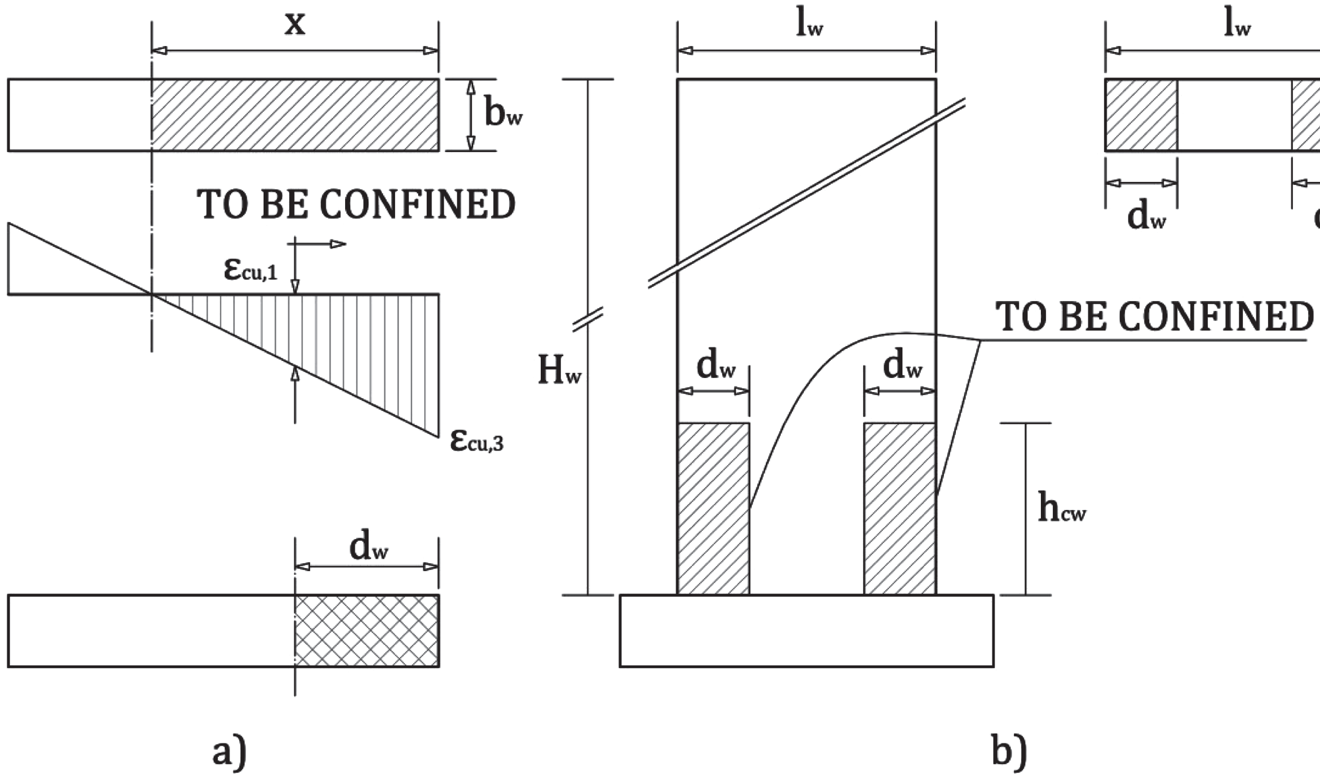

Fig. 3. *Regions to be laterally prestressed in a RC shear wall: a) horizontal cross-section; b) vertical cross-section.*
Zone da confinare di pareti di controvento in c.a.: a) sezione orizzontale; b) sezione verticale.

load-carrying capacity of I-shaped RC elements subject to multiaxial precompression.

The remainder of the paper is organized as follows. We describe in Sect. 2 the adopted constitutive laws for concrete, under triaxial stress states, and ordinary and high-strength steel rebars. Next, we present a variety of design charts (Sect. 3), and moment-curvature diagrams (Sect. 4) of laterally prestressed I-beams, examining different cross-section geometries, lateral prestress ratios, longitudinal prestrain levels, and steel reinforcement ratios. The given results emphasize the special ability of the lateral prestress technique in enhancing both strength and ductility properties of the examined RC elements, even under moderately large lateral prestress of the cross-section flanges. The main conclusions and future research developments are proposed in Sect. 5.

2. **Material and cross-section modeling**

Let us examine the mechanical response of a I-shaped concrete member with respect to an orthogonal reference frame x_1, x_2, x_3, which has the x_1 and x_2 axes aligned with the principal directions of the cross-section (x_1 parallel to the flanges, and x_2 parallel to the web), and the x_3 axis aligned with the member axis. Such an element is subject to constant lateral prestresses σ_1 and σ_2, and is equipped with ordinary steel rebars along the web, and high-strength steel rebars along the flanges. The latter might eventually be (longitudinally) prestressed, in order to apply a fully 3D prestress state to the member under consideration.

The constitutive response of the different elements composing such a member (concrete and reinforcing steel bars) are first modeled. The overall cross-section response is then described.

2.1. *Failure surface of concrete*

Assuming isotropic behavior, the failure (or yield) surface of concrete under triaxial stress states can be drawn in the 3D Haigh-Westergaard space of the principal stresses, $\sigma_1, \sigma_2, \sigma_3$ and characterized through [Ferrara et al., 1977; Ottosen, 1979; Bigoni and Piccolroaz, 2004; Higgins et al., 2013; Gupta, 2013; Liolios and Exadaktylos, 2013]

– "deviatoric" sections with planes orthogonal to the hydrostatic axis $\sigma_1 = \sigma_2 = \sigma_3$ (deviatoric planes, Fig. 4);

– "meridian" sections with Rendulic planes [Ferrara et al., 1977] (shear stress-mean stress planes, see Fig. 5).

Such a surface is usually described in terms of the first invariant of the stress tensor, and the second and third invariants of the deviatoric stress tensor, i.e. the quantities

$$I_{1\sigma} = \sigma_1 + \sigma_2 + \sigma_3; \; J_{2\sigma} = \frac{1}{2}(\bar{\sigma}_1^2 + \bar{\sigma}_2^2 + \bar{\sigma}_3^2); \quad J_{3\sigma} = \bar{\sigma}_1\bar{\sigma}_2\bar{\sigma}_3 \tag{1}$$

where

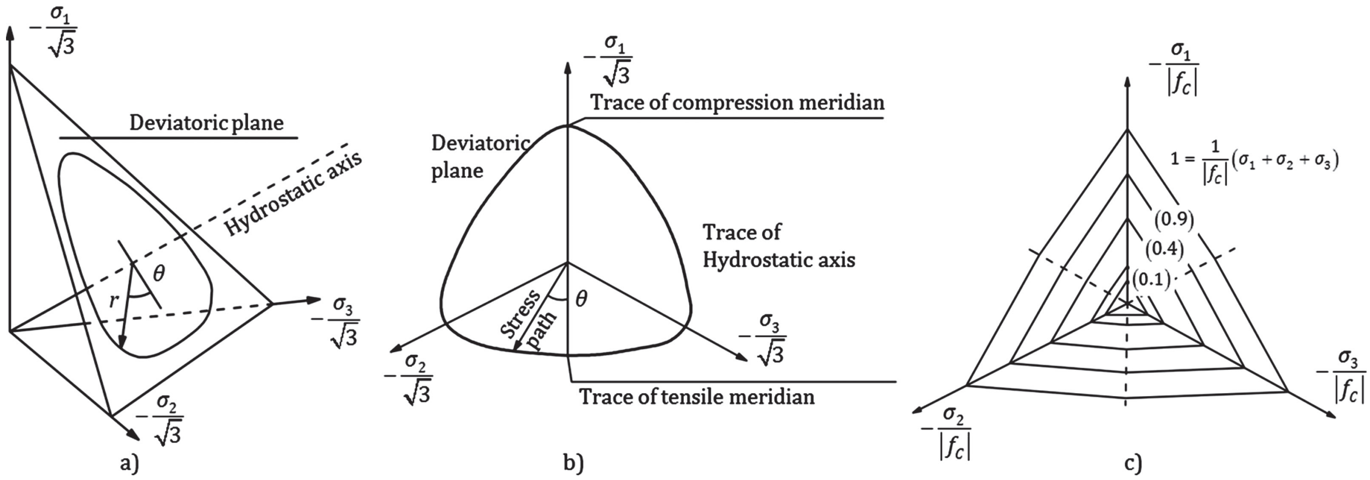

Fig. 4. *a) current deviatoric section of the failure surface; b) deviatoric section far away from the origin of the principal stress space; c) deviatoric section close to the origin of the principal stress space.*
a) sezione deviatorica corrente della superficie di resistenza; b) sezione deviatorica distante dall'origine dello spazio delle tensioni principali; c) sezione deviatorica prossima all'origine dello spazio delle tensioni principali.

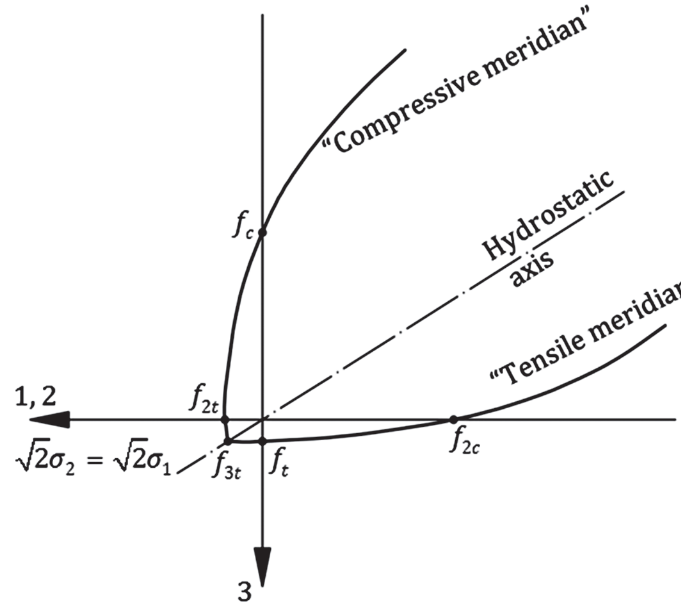

Fig. 5. *Longitudinal section of the failure surface with a Rendulic plane.*
Sezione longitudinale della superficie di resistenza con un piano di Rendulic.

$$\bar{\sigma}_1 = \sigma_1 - \sigma_{\text{oct}}$$

$$\bar{\sigma}_2 = \sigma_2 - \sigma_{\text{oct}} \qquad \sigma_{oct} = \frac{I_{1\sigma}}{3} \tag{2}$$

$$\bar{\sigma}_3 = \sigma_3 - \sigma_{\text{oct}}$$

A popular yield criterion for concrete has been formulated by [Ottosen, 1977], assuming (Figs. 4,5):

– the failure surface is smooth and convex everywhere, except at the vertex;

– the meridians are parabolic;

– the deviatoric sections switch from quasi-triangular to circular, as the hydrostatic stress increases.

The yield locus formulated by Ottosen depends on four dimensionless parameters (A, B, K_1, K_2) and is defined through the scalar equation

$$\frac{AJ_{2\sigma}}{|f_c|^2} + \lambda\frac{J_{2\sigma}}{|f_c|} + \frac{BI_{1\sigma}}{|f_c|} - 1 = 0 \tag{3}$$

where

$$\lambda = \begin{cases} K_1\cos\left[\frac{1}{3}ar\cos(K_2\cos 3\theta)\right] & if \;\; \cos 3\theta \geq 0 \\ K_1\cos\left[\frac{\pi}{3} - \frac{1}{3}ar\cos(-K_2\cos 3\theta)\right] & if \;\; \cos 3\theta < 0 \end{cases} \tag{4}$$

$$\cos 3\theta = \left(3\frac{\sqrt{3}}{2}\right)\left(\frac{J_{3\sigma}}{J_{2\sigma}^{3/2}}\right) \tag{5}$$

Tab. 1. *Available strength parameters of concrete.*
Parametri di resistenza del calcestruzzo.

	[Schickert and Winkler, 1977]	[Linse and Aschl, 1976]
1) uniaxial compressive strength $\lvert f_C \rvert$	30.6 MPa	31.3 MPa
2) $K = f_t / \lvert f_C \rvert$	0.10	0.10
3) biaxial compressive strength $\lvert f_{2C} \rvert$	1.21 $\lvert f_C \rvert$	1.16 $\lvert f_C \rvert$
4) σ_{oct}, τ_{oct}	–88.3 MPa, 57.9 MPa	–50.0 MPa, 43.6 MPa

Tab. 2. *Ottosen parameters.*
Parametri di Ottosen.

Data	*A*	*B*	K_1	K_2
[Schickert and Winkler, 1977]	3.2244	3.4555	11.1538	0.9962
[Linse and Aschl, 1976]	2.1272	3.2965	11.5006	0.9900

By definition, the parameters (A, B, K_1) are positive, and it results $0 \le K_2 \le 1$. Such quantities can be experimentally determined through the following laboratory tests:

– uniaxial compression, giving the uniaxial compression strength f_C;

– uniaxial tension, providing the uniaxial tensile strength f_t, and the strength ratio $K = f_t / \lvert f_C \rvert$;

– uniform biaxial compression, giving the uniform biaxial compressive strength f_{2C};

– failure test at a given stress state along the compressive meridian, providing the quantities: $\sigma_{oct} / \lvert f_C \rvert$ and $\tau_{oct} / \lvert f_C \rvert$, where σ_{oct} and τ_{oct} are the octahedral normal and shear stresses, respectively ($\sigma_{oct} = I_{1\sigma}/3$, $\tau_{oct} = \sqrt{2/3 J_{2\sigma}}$).

Table 1 and Table 2 show experimental values of the above quantities, and the associated Ottosen's parameters, obtained by [Schickert and Winkler, 1977] (used for the simulations presented in the Sects. 3 and 4), and [Linse and Aschl, 1976].

2.2. *Stress-strain response of concrete*

Let us consider now the stress-strain response of an infinitesimal element of a laterally prestressed concrete member, assuming strain and stress components positive if the material is compressed. We assume that the lateral prestresses σ_1 and σ_2 remain constant during loading, and let the axial strain ε_3 increase up to axial failure.

For what concerns the compressive branch of the axial stress-strain law (σ_3 vs ε_3), we discard Poisson's effect ($\nu \approx 0$), and make use of the constitutive law proposed by [Ottosen, 1979], which naturally complements the failure surface discussed in the previous section. Other models of the same (secant) type have been proposed by [Cedolin and Mulas, 1971], and [Cedolin et al., 1977]. Ottosen's constitutive model depends on the following quantities:

– initial value of the Young modulus E_0;

– uniaxial compressive and tensile strengths f_C and f_t;

– "softening" parameter D, which characterizes the slope of the softening branch of the stress-strain response;

– "nonlinearity" factor β defined as follows

$$\beta = \frac{\sigma_3}{\sigma_{3f}} \tag{6}$$

where:

– σ_3 is the current maximum compressive stress;

– σ_{3f} is the corresponding failure stress.

The conditions: $0 \le \beta \le 1$, $\beta = 1$, and $\beta > 1$, respectively define stress states lying inside, on the boundary, and outside the failure surface. Ottosen's law for the secant Young modulus of concrete is the following

$$E_S = \frac{1}{2}E_O - \beta\left(\frac{1}{2}E_O - \bar{E}_f\right) \pm + \sqrt{\left[\frac{1}{2}E_O - \beta\left(\frac{1}{2}E_O - \bar{E}_f\right)\right]^2 + \bar{E}_f^2 \beta [D(1-\beta) - 1]} \tag{7}$$

where positive and negative signs respectively apply to the ascendant and softening branches of the stress-strain curve. In Equation (7), $\bar{E}_f$ denotes the failure value of E_s, which is defined through

$$\bar{E}_f = \frac{E_C}{[1 + (4(\alpha - 1)k)]} \tag{8}$$

Here, E_c denotes the failure value of E_s under uniaxial compression, and it results

$$k = \left(\frac{\sqrt{J_{2\sigma}}}{\lvert f_C \rvert}\right)_f - \frac{1}{3}, \tag{9a}$$

$$\alpha = \frac{E_O}{E_C}. \tag{9b}$$

where $\left(\sqrt{J_{2\sigma}}\right)_f$ denotes the failure value of the second invariant of the deviatoric stress tensor. For $k < 0$, the result $\bar{E}_f = E_c$ applies.

For what concerns the tensile branch of the σ_3 vs ε_3 response, we assume the tension-stiffening behavior illustrated in Fig. 6 [Belarbi and Hsu, 1994].

The overall longitudinal response of the laterally prestressed element is composed of the following branches

$$\sigma_3 = \frac{\left[E_0 + \bar{E}_f^2 \frac{\varepsilon_3}{\sigma_{3f}}(D-1)\right]}{\left[1 + 2\frac{\varepsilon_3}{\sigma_{3f}}\left(\frac{1}{2}E_0 - \bar{E}_f\right) + \bar{E}_f^2 D \frac{\varepsilon_3^2}{\sigma_{3f}^2}\right]}\varepsilon_3$$

$$\varepsilon_{3u} \le \varepsilon_3 \le 0 \tag{10}$$

$$\sigma_3 = E_0 \varepsilon_3 - \left(2E_0 \varepsilon_{tf} - 3f_t\right)\left(\frac{\varepsilon_3}{\varepsilon_{tf}}\right)^2 + + \left(E_0 \varepsilon_{tf} - 2f_t\right)\left(\frac{\varepsilon_3}{\varepsilon_{tf}}\right)^3$$

$$0 \le \varepsilon_3 \le \varepsilon_{tf} \tag{11}$$

$$\sigma_3 = f_t \qquad \varepsilon_{tf} \le \varepsilon_3 \le \varepsilon_{tu} \tag{12}$$

$$\sigma_3 = \frac{\bar{\varepsilon}_t}{\varepsilon_3}\bar{\sigma}_t \qquad \varepsilon_3 > \varepsilon_{tu} \tag{13}$$

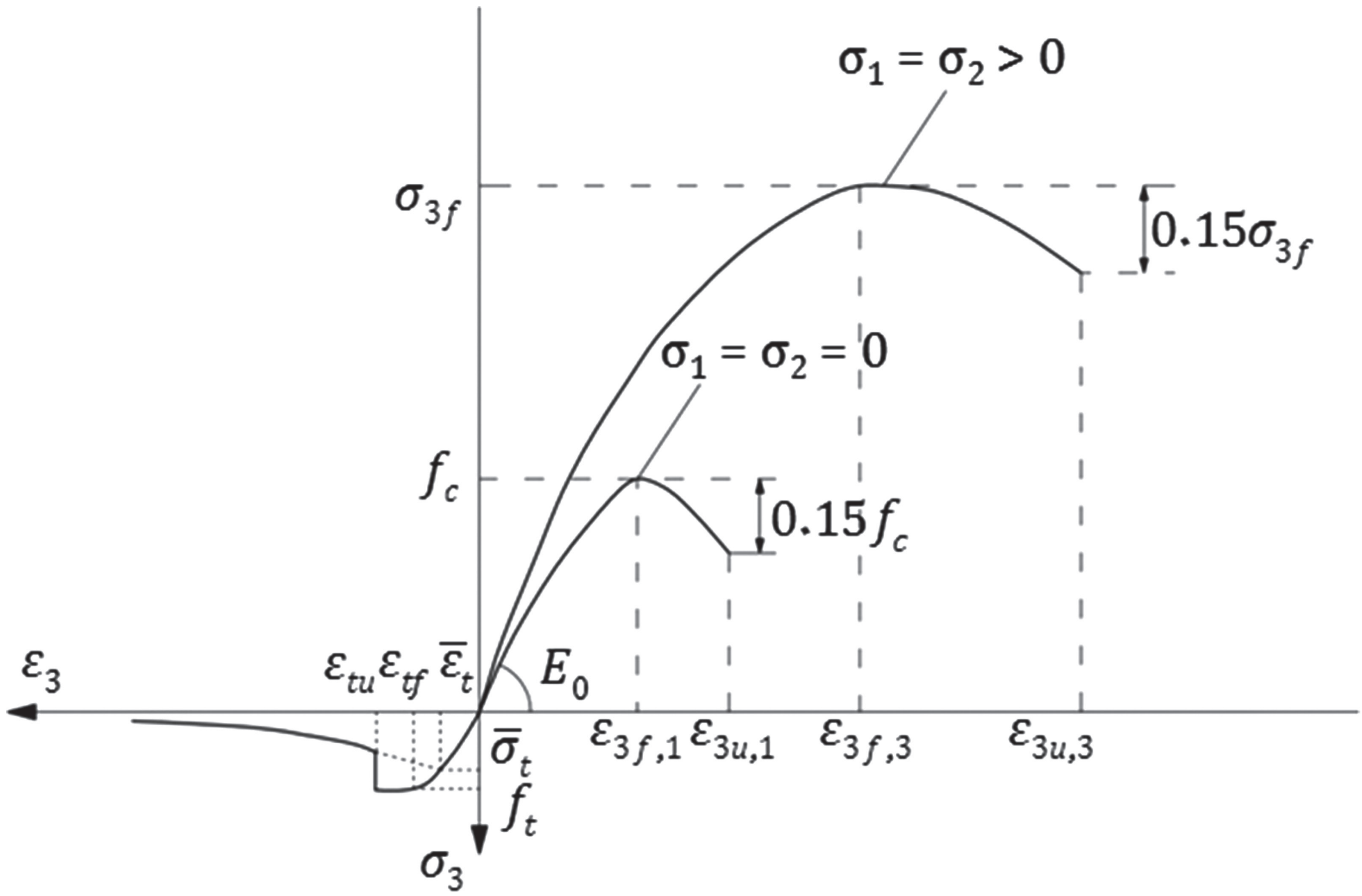

Fig. 6. *Longitudinal stress-strain response of a laterally prestressed concrete element [Ottosen, 1979].*
Risposta longitudinale tensione-deformazione di elementi in calcestruzzo confinati lateralmente [Ottosen, 1979].

Tab. 3. *Adopted constitutive parameters of concrete.*
Parametri costitutivi adottati per il calcestruzzo.

$E_0 = 2.84 \times 10^4 MPa$	$D = 0.2$	$\beta_0 = \beta_1 = \beta_2 = 1$
$\varepsilon_{cf1} = 0.00197$	$\varepsilon_{3f,1} = 0.3\%$	$\varepsilon_{tf} = \varepsilon_{tu} = 0.014\%$

The numerical results presented in the following sections are based on the above constitutive laws, and the material parameters provided in Table 3.

2.3. *Stress-strain response of reinforcing steel bars*

The adopted constitutive laws for the high-strength ("p") and ordinary ("f") steel bars are shown in Fig. 6a and Fig. 6b respectively. Let ε_p and σ_p respectively denote the longitudinal strain and longitudinal stress acting in the generic high-strength bar, and let ε_f and σ_f respectively denote the longitudinal strain and longitudinal stress acting in the current ordinary steel bar. For the high-strength rebars we make use of the Ramberg-Osgood constitutive model [Ramberg and Osgood, 1943], which is defined through (Fig. 7a)

$$\sigma_p = E_p \varepsilon_p \qquad |\varepsilon_p| < \varepsilon_{pe} \tag{14}$$

$$\varepsilon_p = \frac{\sigma_p}{E_p} + e_{pp}\left[\frac{|\sigma_p| - |\sigma_{pe}|}{\sigma_{pp} - \sigma_{pe}}\right]^n \frac{\sigma_p}{|\sigma_p|} \quad \varepsilon_{pe} < |\varepsilon_p| < \varepsilon_{pf} \tag{15}$$

where:
- E_p is the Young modulus of "p" bars;
- σ_{pp} is the yield stress of "p" bars;
- e_{pp} is the strain corresponding to σ_{pp};
- (σ_{pe}, ε_{pe}) are the coordinates of the final point of linear elastic branch;
- (σ_{pf}, ε_{pf}) are the coordinates of the failure point;
- n is a prescribed exponent.

For what concerns the ordinary steel bars, we instead make use of the stress-strain response defined by the following branches (Fig. 7b) [Park and Paulay, 1975]

$$\sigma_f = E_f \varepsilon_f \qquad |\varepsilon_f| < \varepsilon_{fy} \tag{16}$$

$$\sigma_f = \sigma_{fy} \frac{\varepsilon_f}{|\varepsilon_f|} \qquad \varepsilon_{fy} < |\varepsilon_f| < \varepsilon_{fh1} \tag{17}$$

$$\sigma_f = \left[\sigma_{fy} + E_{fh}\left(|\varepsilon_f| - \varepsilon_{fh1}\right)\right]\frac{\varepsilon_f}{|\varepsilon_f|} \quad \varepsilon_{fh1} < |\varepsilon_f| < \varepsilon_{fh2} \tag{18}$$

$$\sigma_f = \sigma_{ff} \frac{\varepsilon_f}{|\varepsilon_f|} \qquad \varepsilon_{fh2} < |\varepsilon_f| < \varepsilon_{fu} \tag{19}$$

where:
- E_f is the Young modulus of "f" bars;
- E_{fh} is the slope of the hardening branch;
- (σ_{fy}, ε_{fy}) are the coordinates of the final point of the linear elastic branch;

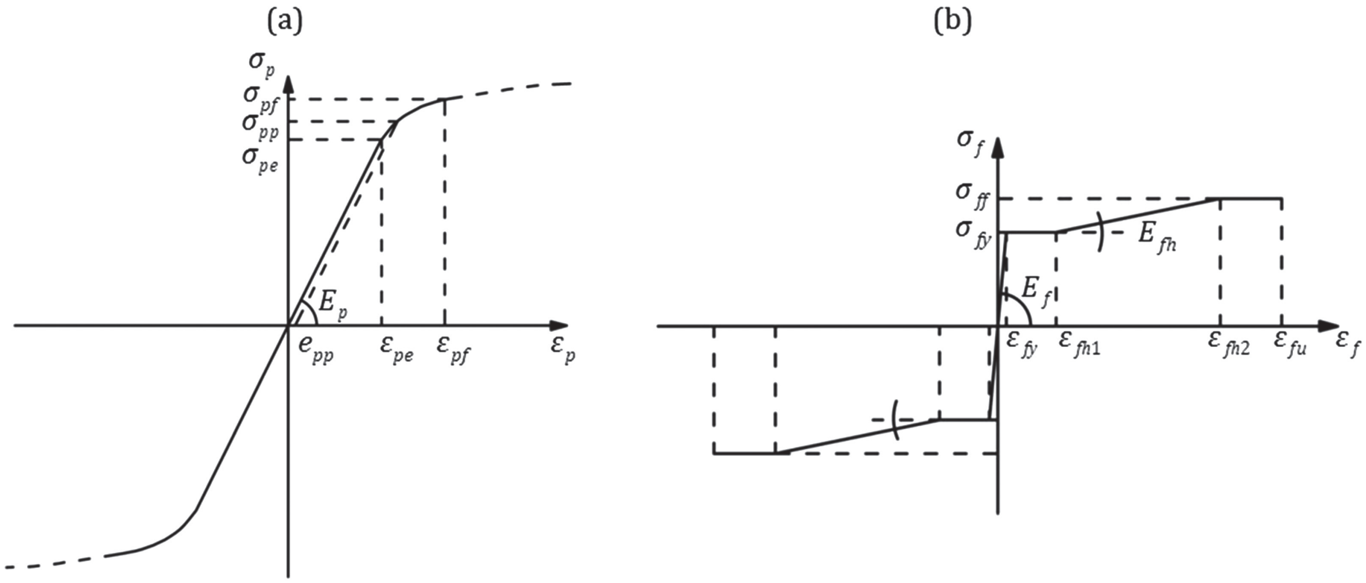

Fig. 7. *Adopted constitutive laws for reinforcing steel bars: a) high-strength rebars; b) ordinary rebars.*
Leggi costitutive adottate per le armature di rinforzo: a) barre di acciaio ad alta resistenza; b) barre di acciaio ordinario.

Tab. 4. *Material parameters employed for high-strength rebars.*
Parametri costitutivi adottati per le armature ad alta resistenza.

$\sigma_{pf}/\lvert f_C\rvert = 30$	$\sigma_{pp}/\sigma_{pf} = 0.667$	$\sigma_{pe}/\sigma_{pp} = 0.700$
$E_p/\sigma_{pf} = 233$	$\varepsilon_{pf} = 8\%$	$e_{pp} = 0.2\%$

Tab. 5. *Material parameters employed for ordinary rebars.*
Parametri costitutivi adottati per le armature ordinarie.

$\sigma_{fy}/\lvert f_C\rvert = 15$	$\sigma_{ff}/\sigma_{fy} = 1.5$	$\varepsilon_{fy} = 0.2\%$
$\varepsilon_{fh} = 1.0\%$	$\varepsilon_{fh2} = 10\%$	$\varepsilon_{fu} = 20\%$

– ε_{fh1} and ε_{fh2} are the strains associated with the initial and final points of the hardening branch;

– $(\sigma_{ff}, \varepsilon_{fu})$ are the coordinates of the failure point.

The simulations presented in Sects. 3 and 4 make use of the above constitutive models, and the numerical data provided in Table 4 and Table 5.

2.4. *Cross-section modeling*

Let us now consider the overall response of the current cross-section (Fig. 8c), under the action of an axial load N, and a bending moment M about the x_1 axis. We refer our analysis to the following dimensionless quantities

$$\nu = \frac{N}{A_c\lvert f_c\rvert}, \qquad \mu = \frac{M}{A_c l_w \lvert f_c\rvert}, \tag{20}$$

where A_c denotes the concrete cross-section area.

The present modeling of the cross-section response is based on the following assumptions:

– all the materials are isotropic and homogeneous;

– the cross-sections remains plane and unstretched during deformation;

– there is perfect adhesion at the steel-concrete interface;

which lead us to the ultimate strain profiles shown in Fig. 8b, describing all the possible failure modes of the cross-section: (1: tension failure; 2: balanced failure; 3&4: compression failure).

3. **Design charts of laterally prestressed members**

We provide in the present section interaction diagrams plotting the dimensionless ultimate axial load $\nu = N/(A_c\lvert f_c\rvert)$ against the dimensionless ultimate bending moment $\mu = M/(A_c l_w \lvert f_c\rvert)$. Such diagrams have been numerically computed on the basis of the constitutive assumptions introduced in the previous section (Fig. 9). Referring to the cross-section scheme shown in Fig. 9a, we agree to neglect the tensile branch of the concrete stress-strain response (Fig. 6), and to make use of the following aspect ratio

$$t = t_1 = t_2 = \frac{l_w}{10}, \tag{21}$$

where l_w denotes the web height. We also consider the following values of the flange widths (see Figs. 9 b-e)

$$A = A_1 = A_2 = \left[\frac{l_w}{10},\ \frac{l_w}{3},\ \frac{l_w}{2},\ l_w\right], \tag{22}$$

and four different values of the lateral prestress

$$\sigma_c = \sigma_{c1} = \sigma_{c2} = [0,\ 0.10 f_c,\ 0.20 f_c,\ 0.33 f_c]. \tag{23}$$

Finally, we analyze the following reinforcement ratios

$$\frac{A_p}{A_c} = \frac{A_{p1}}{A_c} = \frac{A_{p2}}{A_c} = 0.00375, \quad \frac{A_f}{A_c} = 0.0025 \tag{24}$$

and three different longitudinal prestrain values of the flange rebars

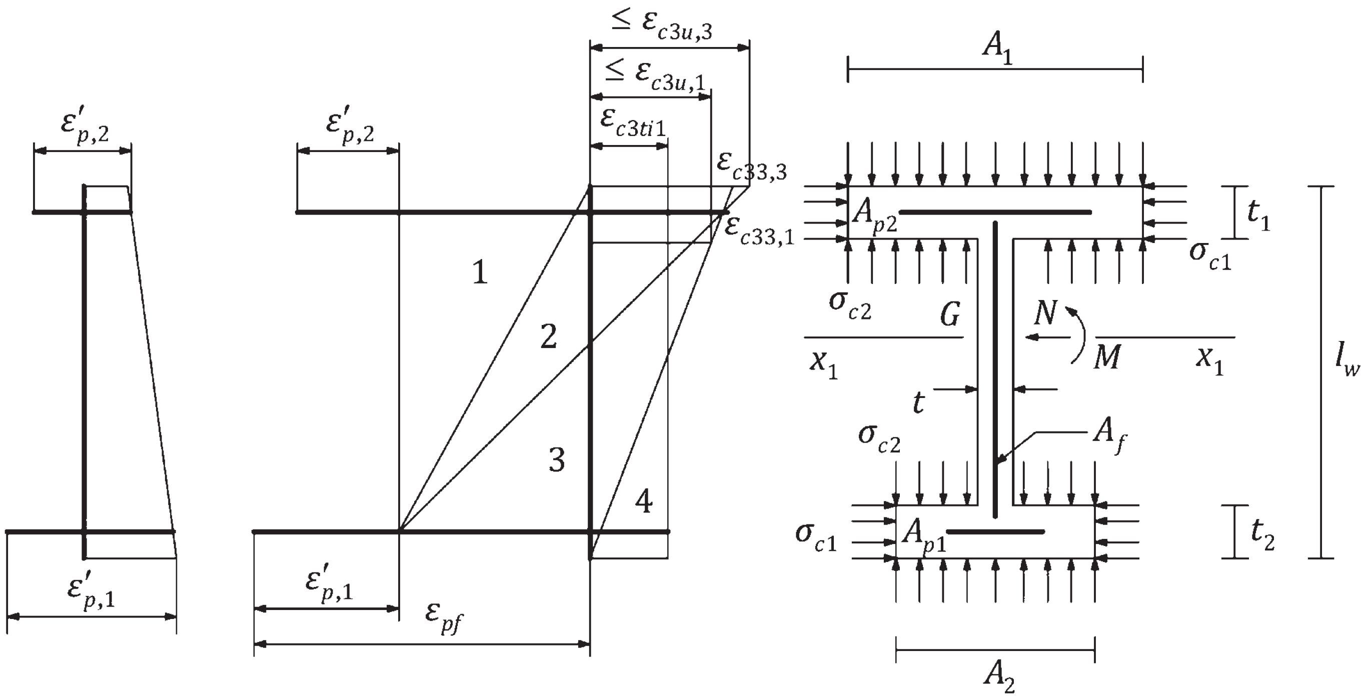

Fig. 8. *Noticeable cross-section strain profiles: a) strain profiles after the prestress of "p" bars; b) ultimate strain profiles; c) cross-section layout.*
Diagrammi di deformazione notevoli sulla sezione retta: a) diagrammi di deformazione a seguito della pretensione delle armature ad alta resistenza; b) diagrammi di deformazione a rottura; c) schema geometrico della sezione trasversale.

$$\varepsilon_p^* = [0,\ 0.0026,\ 0.0050]. \tag{25}$$

The design charts shown in Figs. 9 b-e highlight the influences of the aspect ratio A/l_w and the lateral prestress level σ_c/f_c on the ν-μ limit domain. We observe that such a domain significantly expands in the direction of positive ν values, as the flange width and the lateral prestress level increase. On the contrary, increasing values of the longitudinal prestrain ε_p^* produce a contraction of such a domain in the same direction (Fig. 9f).

4. **Moment – curvature diagrams**

We now examine moment-curvatures diagrams relating the dimensionless bending moment μ to the dimensionless curvature χ (we let χ^{l_w} denote the cross-section curvature). Such a study is conducted on accounting for the tensile branch of the stress-strain curve of concrete shown in Fig. 6. We consider the following values of the dimensionless axial force

$$\nu = [0.10,\ 0.25,\ 0.50,\ 0.70] \tag{26}$$

and different values of the design variables introduced in the previous section (see Figs. 10 and 11). Figs. 10 a-d show the μ-χ^{l_w} curves of sections with aspect ratio $A/l_w = 1/2$ (medium flange I-beam); while Figs. 10 e-h display the analogous curves of sections with $A/l_w = 1/3$ (narrow flange I-beam). Figures 11 a-d present the μ-χ^{l_w} curves of sections with $A/l_w = 1$ (wide flange I-beam, or W-beam), for given reinforcement ratios ($A_p/A_c = 0.00375$, $A_f/A_c = 0.0025$). Finally, Figs. 11 e-h show the moment – curvature curves of medium flange I-beams with $A_f/A_c = 0.0025$, and different values of the flange reinforcement ratio A_p/A_c (Fig. 8). The results in Figs. 10 and 11 a-d highlight that the cross-section rotation ductility remarkably grows with the lateral prestress level σ_c/f_c. Such a beneficial effects of the lateral prestress becomes less remarkable in presence of large values of the dimensionless axial force ν. By increasing the flange reinforcement ratio A_p/A_c, we observe a slight decrease of the cross-section ductility, which is balanced by an appreciable increase in the ultimate bending capacity (Figs. 11 e-h).

5. **Concluding remarks**

We have presented a parametric study on the beneficial effects of active lateral and longitudinal prestress states on the ultimate axial load – bending moment interaction diagrams, and moment-curvature curves of RC I-beams. The numerical results presented in Sects. 3 and 4 have shown that the lateral prestress of the flanges of such elements is able to significantly enhance both the ultimate strength and ductility properties of the cross-sections, especially in the case of wide-flange beams. The curvature ductility of laterally prestressed elements gets particularly large in presence of high lateral prestress σ_c/f_c; low or moderately low dimensionless axial loads $\nu = N/(A_c\,|f_c|)$; and weakly reinforcement ratios.

It is worth remarking that the lateral prestress locally enhances the strength and ductility properties of com-

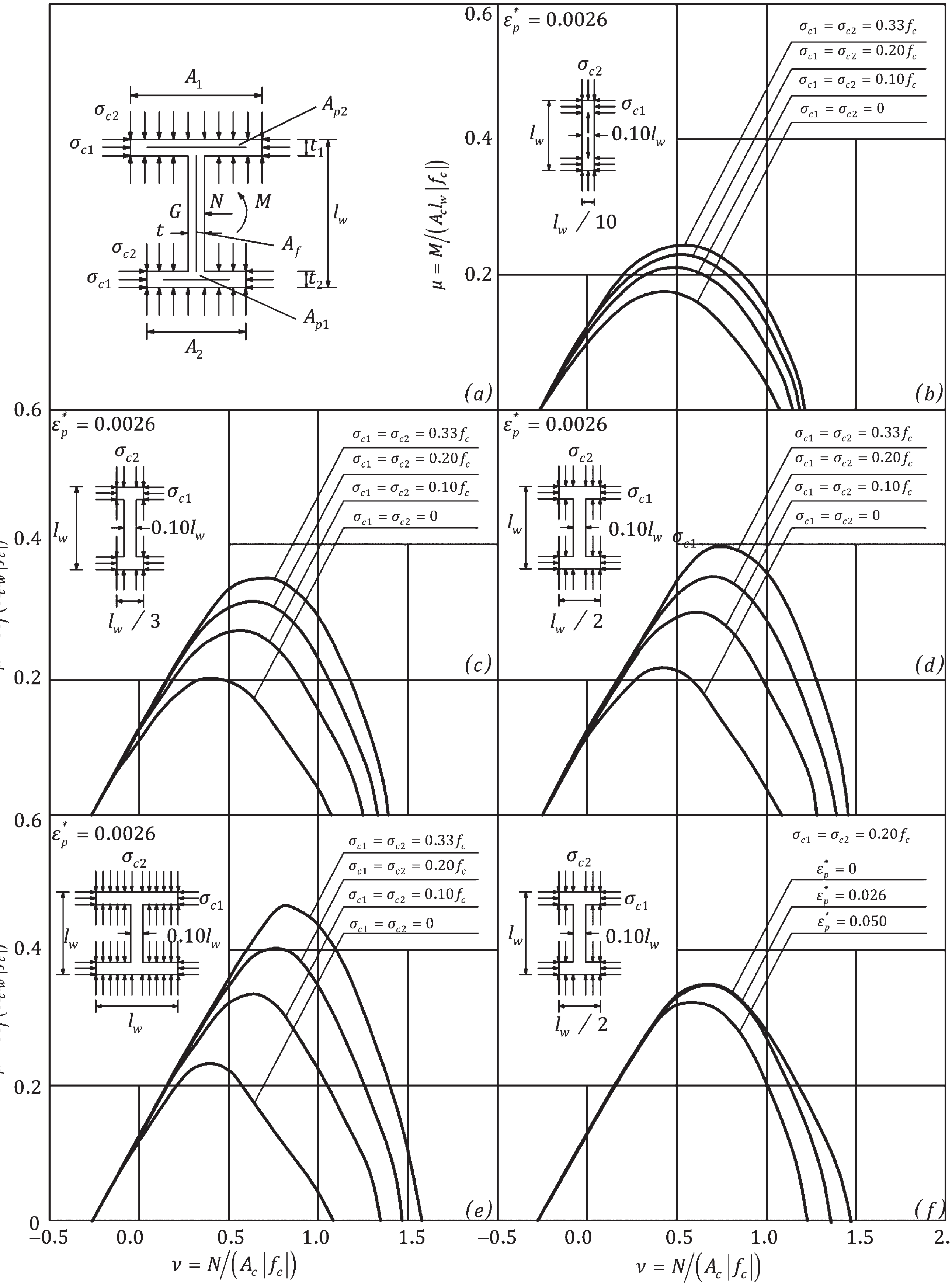

Fig. 9. *Design charts of laterally prestressed I-beams for different cross-section geometries, lateral prestress values and longitudinal prestrains.*
Domini di resistenza di una sezione a doppio T con ali presollecitate lateralmente e longitudinalmente, in corrispondenza di diverse geometrie della sezione trasversale e diversi valori delle precompressioni laterali e longitudinali.

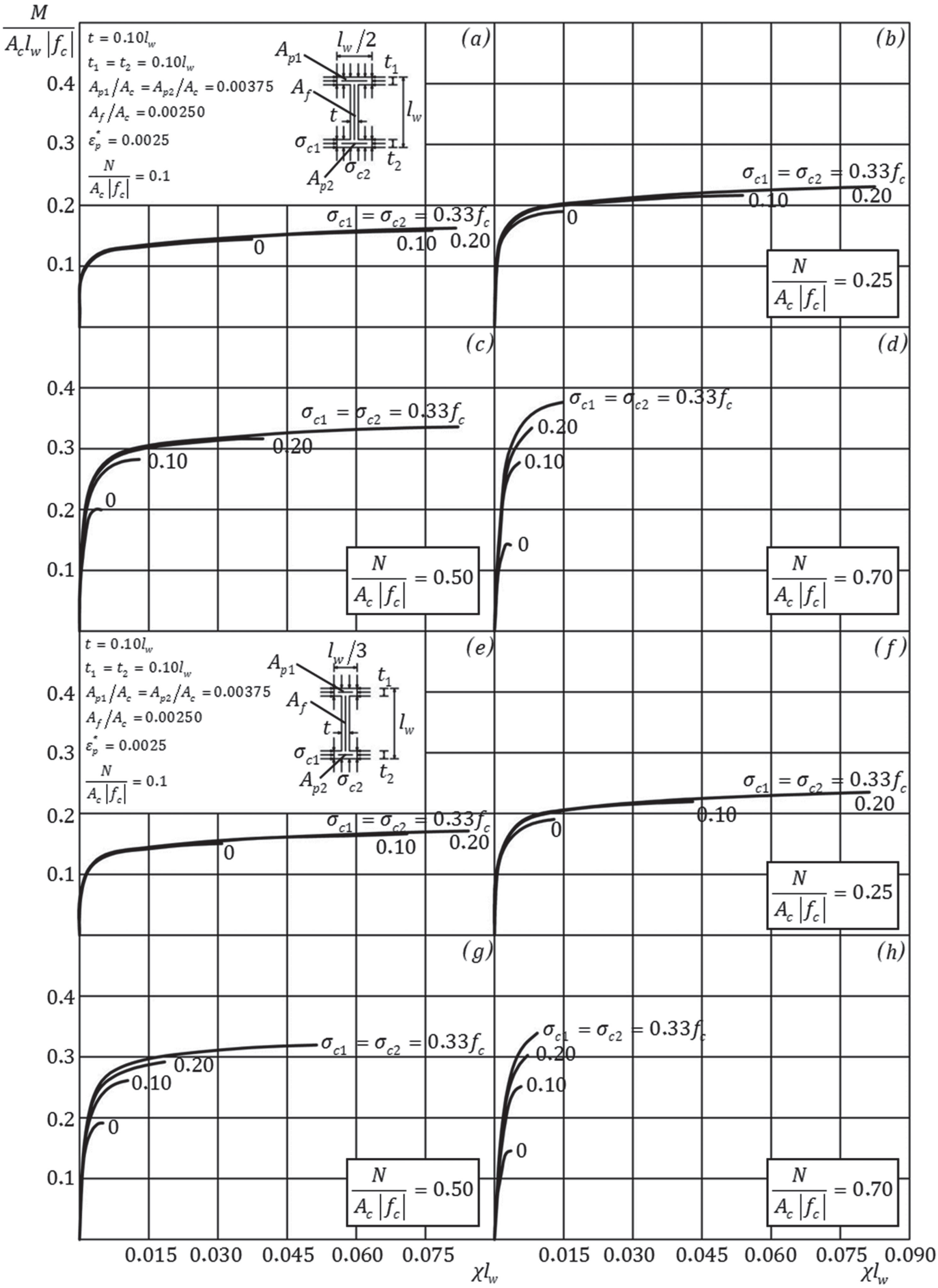

Fig. 10. *Dimensionless bending moment (μ) vs. dimensionless curvature (χl_w) curves of RC I-beams, for different cross-section geometries, lateral prestress values and axial loads.*

Curve momento adimensionale (μ) - curvatura adimensionale (χl_w) di travi a doppio T in c.a., per diverse geometrie della sezione trasversale e diversi valori della precompressione laterale e dello sforzo assiale.

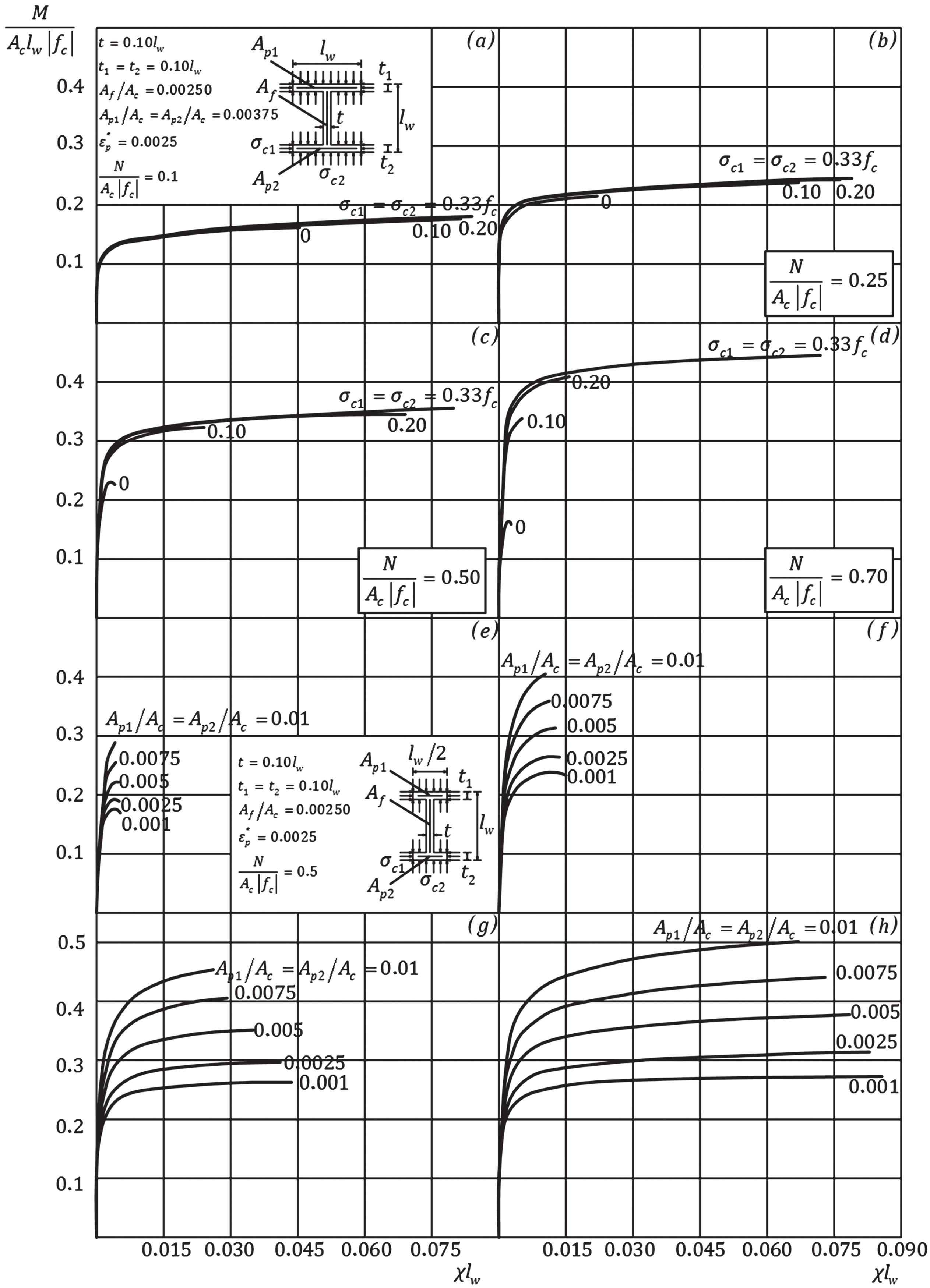

Fig. 11. *Dimensionless bending moment (μ) vs. dimensionless curvature (χl_w) curves of RC I-beams, for different cross-section geometries, lateral prestress values; axial loads; and steel reinforcement ratios.*
Curve momento adimensionale (μ) - curvatura adimensionale (χl_w) di travi a doppio T in c.a., per diverse geometrie della sezione trasversale e diversi valori della precompressione laterale, dello sforzo assiale e dei rapporti di armatura.

pressed concrete (Sect. 2), and additionally modifies the failure mechanism of the cross-section, by reducing the neutral axis depth at the ultimate limit state (Fig. 8). Furthermore, the improved strength properties of the laterally prestressed concrete lead to an increase in the maximum reinforcing steel area ensuring ductile failure of the cross-section (with the tension steel yielding), as compared to passively confined members.

Overall, we conclude that the amplitude of the lateral prestress can be looked at as a new design variable of seismic resistant RC elements, such as, e.g., structures of RC buildings and bridges in seismically active areas, to be suitably tuned through an optimized design of the zones to be laterally prestressed, and the magnitude of the lateral prestress.

We address the enlargement of the parametric study presented in Sects. 3 and 4 to future work. Another challenging generalization of the current research regards the study of the serviceability limit state on crack width of prestressed RC elements, to be conducted on combining the constitutive assumptions introduced in the present work with variational fracture models [Fraternali, 2007; Schmidt et al., 2009; Fraternali et al., 2010]. Additional future extensions of the present study might regard the mechanics of sandwich structures incorporating prestressed layers [Mortazavi et al., 2003; Mukherjee and Rai, 2009; El Sayed et al., 2009], as well as the use of mesh-free methods; tensegrity networks and strut-and-tie models for the optimal design of spatially precompressed RC and masonry structures [Fraternali et al., 2011; Fraternali et al., 2002; Fraternali, 2010; Fraternali, 2011; Fraternali et al., 2012a, b; Skelton et al., 2013].

Acknowledgments

The authors acknowledge financial support from the Italian Ministry of Foreign Affairs through the Science and Technology Cooperation Program between Italy and USA (years 2014-2015), grant US14GR08.

References

/1/ Belarbi, A., and Hsu, T.T.C. [1994] "Constitutive Laws of Concrete in Tension and Reinforcing Bars Stiffened by Concrete", *ACI Structural Journal*, **91(4)**, 465-474.

/2/ Bigoni, D., and Piccolroaz, A. [2004] "Yield criteria for quasibrittle and frictional materials", *International Journal of Solids and Structures*, **41(11)**, 2855-2878.

/3/ Cedolin, L., Crutzen, Y.R.J., De Poli, S. [1977] "Triaxial Stress-Strain Relationship for Concrete", *Journ. Eng. Mech. Div. ASCE*, **103 EM3**, 423-439.

/4/ Cedolin, L., and Mulas, M.G. [1971] "Una legge costitutiva secante ed esplicita per il calcestruzzo in stati piani di tensione", *Studi e ricerche Politecnico di Milano*, **3**, 75-105.

/5/ El Sayed, T., Mock, W., Mota, A., Fraternali, F., Ortiz M. [2009] "Computational Assessment of Ballistic Impact on a High Strength Structural Steel/ Polyurea Composite Plate", *Computational Mechanics*, **43(4)**, 525-534. ISSN: 0178-7675 (Print) 1432-0924 (Online). DOI: 10.1007/s00466-008-0327-6.

/6/ Ferrara, G., Rossi, P, Rossi, P.P., Ruggeri, L. [1977] "Dispositivi di prova per l'analisi sperimentale del comportamento di conglomerati cementizi sottoposti a stati triassiali di sollecitazione", *ISMES*, Bergamo, Italy.

/7/ Fraternali, F. [2007] "Free discontinuity finite element models in two-dimensions for in-plane crack problems", *Theor. Appl. Fract. Mec.*, **47**, 274-282.

/8/ Fraternali. F. [2010] "A Thrust Network Approach to the Equilibrium Problem of Unreinforced Masonry Vaults via Polyhedral Stress Functions", *Mechanics Research Communications*, **37**, 198-204. ISSN: 0093-6413, DOI:10.1016/j.mechrescom.2009.12.010.

/9/ Fraternali. F. [2011] "A Mixed Lumped Stress – Displacement Approach to the Elastic Problem of Masonry Walls", *Mechanics Research Communications*, **38**, 176-180. ISSN: 0093-6413, DOI:10.1016/j.mechrescom.2011.03.008.

/10/ Fraternali, F., Angelillo, M., Fortunato, A. [2002] "A Lumped Stress Method for Plane Elastic Problems and the Discrete-Continuum Approximation", *International Journal of Solids and Structures*, **39**, 6211-6240. ISSN: 0020-7683.

/11/ Fraternali, F., Marino, A., Elsayed, T., Della Cioppa, A. [2011] "On the structural shape optimization via variational methods and evolutionary algorithms", *Mechanics of Advanced Materials and Structures*, **18**, 225-243. ISSN: 1537-6494, DOI: 10.1080/15376494.2010.483319.

/12/ Fraternali, F., Negri, M., Ortiz, M. [2010] "On the Convergence of 3D Free Discontinuity Models in Variational Fracture", *Int. J. Fract.*, **166 (1-2)**, 3-11.

/13/ Fraternali, F., Senatore, L., Daraio, C. [2012a] "Solitary waves on tensegrity lattices", *Journal of the Mechanics and Physics of Solids*, **60**, 1137-1144. ISSN: 0022-5096 DOI: 10.1016/j.jmps.2012.02.007.

/14/ Fraternali, F., Lorenz, C.D., and Marcelli, G. [2012b]. On the Estimation of the Curvatures and the Bending Rigidity of Membrane Networks via a local Maximum-Entropy Approach. J. Comput. Phys. 231:528-540.

/15/ Gardner, N.J., Godse, R.M., Wong, T.F. [1992] "Laterally Prestressed Eccentrically Loaded Slender Columns", *Structural Journal*, **89(5)**, 547-554.

/16/ Gupta, P.K. [2013] "Confinement of concrete columns with unplasticized Poly-vinyl chloride tubes", *International Journal of Advanced Structural Engineering*, **5(19)**, 1-8.

/17/ Higgins, L., Forth, J.P., Neville, A., Jones, R., Hodgson, T. [2013] "Behaviour of cracked reinforced concrete beams under repeated and sustained load types", *Engineering Structures*, **56**, 457-465.

/18/ Janke, L., Czaderski, C., Ruth, J., Motavalli, M. [2009] "Experiments on the residual load-bearing

capacity of prestressed confined concrete columns", *Engineering Structures*, **31**, 2247-2256.
/19/ Linse, D., and Aschl, H. [1976] "Versuche zum Verhalten von Beton unter mehrachsiger Beanspruchung", Technische Universitat Munchen Lehrstuhl fur Massivbau.
/20/ Liolios, P., and Exadaktylos, G. [2013] "A smooth hyperbolic failure criterion for cohesive-frictional materials", *International Journal of Rock Mechanics and Mining Sciences*, **58**, 85-91.
/21/ Mortazavi, A.A., Pilakoutas, K., Son K.S. [2003] "RC column strengthening by lateral pre-tensioning of FRP", *Construction and Building Materials*, **17**, 491-497.
/22/ Mukherjee, A., and Rai, G.L. [2009] "Performance of reinforced concrete beams externally prestressed with fiber composites", *Construction and Building Materials*, **23**, 822-828.
/23/ Ottosen, N.S. [1977] "A failure criterion for concrete", *Journ. Eng. Mech, Div. ASCE*, **103**.
/24/ Ottosen, N.S. [1979] "Constitutive Model for Short-Time Loading of Concrete", *Journ. Eng. Mech, Div. ASCE*, **105 EM1**.
/25/ Park, R., and Paulay, T. [1975] "Reinforced concrete structures", John Wiley & Sons, New York.
/26/ Ramberg, W., and Osgood, W.R. [1943] "Description of stress-strain curves by three parameters", Technical Note No. 902, National Advisory Committee For Aeronautics, Washington DC. (http://ntrs. nasa. gov/archive/nasa/casi.ntrs. nasa. gov/19930081614_1993081614. pdf).
/27/ Saadatmanesh H., Ehsani M.R., Jin L. [1997] "Repair of Earthquake-Damaged RC Columns with FRP Wraps", *ACI Structural Journal*, **94-S20**, 206-214.
/28/ Schickert, G, and Winkler, H. [1977] "Versuchsergebnisse zur Festigkeit von Beton bei mehraxialer Druckbeanspruchung", DAfStb Heft 277 Wilhelm Ernst - Sohn.
/29/ Schmidt, B., Fraternali, F., Ortiz, M. [2009] "Eigenfracture: an eigendeformation approach to variational fracture", *Multisc. Model. Sim.*, **7(3)**, 1237-1266.
/30/ Skelton, R.E., Fraternali, F., Carpentieri, G., Micheletti, A. [2013] "Minimum mass design of tensegrity bridges with parametric architecture and multiscale complexity", *Mechanics Research Communications*, Online First. ISSN: 0093-6413, DOI: 10.1016/j. mechrescom.2013.10.017.
/31/ Zaki, M.K. [2013] "Optimal performance of FRP strengthened concrete columns under combined axial-flexural loading", *Engineering Structures*, **46**, 14-27.

Sulla presollecitazione pluriassiale di travi in conglomerato cementizio armato con sezione a doppio T

F. Fraternali, B. Palazzo, G. Carpentieri

Sono ben note, nei problemi di consolidamento strutturale, le tecniche di confinamento laterale di elementi in conglomerato cementizio mediante anelli metallici messi in forza mediante riscaldamento prima del serraggio, staffature metalliche e/o avvolgimenti con materiali polimerici fibro-rinforzati (FRP). Tali tecniche di rinforzo consentono di trasformare lo stato di tensione prevalentemente uniassiale dell'elemento non confinato, che si suppone soggetto all'azione combinata di sforzo normale e momento flettente, in uno stato di tensione pluriassiale, grazie alla pressione laterale di confinamento esercitata dagli elementi trasversali di rinforzo. La presenza di uno stato di sollecitazione triassiale può significativamente incrementare la resistenza del materiale, spostando i cerchi principali di Mohr del tensore delle tensioni verso la zona di maggiore "apertura" della superficie intrinseca del materiale (Fig. 1). Il confinamento "passivo" di elementi in c.a. diventa particolarmente efficace in presenza di importanti deformazioni assiali (ovvero sotto tensioni di compressione vicine alla resistenza ultima del calcestruzzo), presentando, invece, una modesta efficacia in corrispondenza di basse deformazioni assiali, a causa dei modesti valori del coefficiente di Poisson dei calcestruzzi di comune impiego. Sicuramente più efficace è il confinamento "attivo" di membrature in c.a. con sezione retta a doppio T, che può essere ottenuto mediante presollecitazione laterale e longitudinale delle flange (Fig. 2). Tale tecnica di presollecitazione è particolarmente indicata nel caso di nuclei e pareti di controvento di edifici antisismici, nei quali la presenza di stati di compressione biassiali o triassiali può significativamente incrementare le proprietà di resistenza e di duttilità del materiale (Fig. 3).

[Gardener et al., 1992] hanno presentato uno studio teorico-sperimentale sulla resistenza di colonne in c.a. presollecitate lateralmente e soggette ad azioni assiali eccentriche, proponendo una formula empirica per la previsione del carico ultimo di tali elementi. [Zaki, 2013] ha studiato il problema della progettazione ottimale di elementi di confinamento esterni in FRP di colonne in c.a. soggette a sforzo normale e momento flettente, determinando valori ottimizzati di parametri quali lo spessore e la lunghezza delle fasciature in materiale composito. [Saadatmanesh et al., 1997] hanno presentato uno studio sperimentale sul rinforzo con avvolgimenti in FRP di elementi in c.a. danneggiati da azioni sismiche. Le colonne rinforzate con FRP esaminate in questo studio hanno mostrato un netto miglioramento del comportamento isteretico, della resistenza flessionale e della duttilità strutturale, per confronto con gli elementi non rinforzati. [Janke et al., 2009] hanno studiato il comportamento sotto carichi di compressione di elementi cilindrici in calcestruzzo rinforzati con fasce di confinamento pretese in acciaio ed in FRP (fibre di carbonio). I risultati di questo studio hanno dimostrato che la capacità di carico residua degli elementi rinforzati con confinamenti pretesi è significativamente maggiore di quella degli elementi rinforzati con fasciature non pretese, anche in presenza di bassi valori della tensione di pretensione. Il rinforzo e l'adeguamento di membrature in c.a. attraverso fasciature esterne con elementi pretesi in FRP è stato studiato da [Mortazavi et al., 2003] e [Mukherjee and Rai, 2009]. Tali studi hanno mostrato che la pretensione di avvolgimenti in FRP migliora significativamente le proprietà meccaniche del calcestruzzo ed ottimizza altresì l'impiego delle fasciature [Mortazavi et al., 2003], oltre ad incrementare l'entità' dei carichi di progetto in condizioni di servizio ed allo stato limite ultimo (anche più del 100%) [Mukherjee and Rai, 2009].

Il presente studio esamina il comportamento allo stato limite ultimo di travi in conglomerato cementizio armato con sezione a doppio T, che siano presollecitate in direzione trasversale e longitudinale in corrispondenza delle flange e siano soggette all'azione combinata di sforzo normale e momento flettente. Si presenta uno studio parametrico sui domini di resistenza e sui diagrammi momento-curvatura di tali elementi, utilizzando diversi rapporti d'aspetto, livelli di presollecitazione laterale e rapporti d'armatura. Un obiettivo fondamentale del lavoro consiste nello studio dell'influenza di tali variabili di progetto sulla resistenza ultima di elementi in c.a. a doppio T soggetti a stati di sollecitazione pluriassiali. I risultati presentati consentono di concludere che la presollecitazione laterale di confinamento, ancorché applicata alle sole zone terminali della sezione, produce incrementi significativi della resistenza e della duttilità sezionale. Tale incrementi risultano particolarmente sensibili nei casi in cui il meccanismo di rottura della sezione sia dovuto alla crisi locale del calcestruzzo compresso. Il valore della pressione di confinamento laterale di elementi in c.a. si configura, pertanto, come una nuova variabile di progetto, in grado di migliorare contemporaneamente il livello di resistenza e di duttilità della sezione. Per le sue peculiari caratteristiche, il confinamento laterale attivo di elementi strutturali in conglomerato cementizio è particolarmente indicato nel caso delle pareti o dei nuclei verticali di controventamento di edifici destinati ad assorbire elevate azioni sismiche.

L'articolo è organizzato come segue. La Sezione 2 descrive le leggi costitutive adottate per il calcestruzzo, sotto stati di tensione triassiali, e le armature ordinarie e pretese e presenta altresì la modellazione impiegata per descrivere il comportamento a rottura della sezione retta. Le Sezioni 3 e 4 presentano un'ampia casistica di domini di resistenza (Sezione 3) e diagrammi momento-curvatura (Sezione 4) di travi a doppio T soggette a confinamento laterale attivo. Le principali conclusioni e gli sviluppi futuri del presente lavoro sono presentati nella Sezione 5.